Vectorial attosecond transient spectroscopy - Supplementary Information

Noa Yaffe,[1,2] Chen Mor,[1] Nirit Dudovich,[1] and Omer Kneller[1,3]

[1]*Department of Physics of Complex Systems, Weizmann Institute of Science, Rehovot, Israel*

[2]*Email: noa.yaffe@weizmann.ac.il*

[3]*Email: omer.kneller@weizmann.ac.il*

CONTENTS

1. EXPERIMENTAL SETUP

The experimental setup is composed of a co-linear XUV–XUV interferometer with two HHG sources and an interaction cell. A schematic description of the experimental setup is shown in figure 1. A Ti:sapphire laser system with 1-kHz repetition rate delivers IR pulses with 30fs duration at a central wavelength of 800nm. A co-propagating perpendicular second harmonic field (SH) is generated via second-harmonic generation using a 100μm type-I β-barium borate (BBO) crystal. Group-velocity dispersion is compensated using a birefringent calcite crystal, temporally separating the IR and SH pulses. The sub-cycle delay between the fundamental IR and the additional SH field is controlled using a pair of glass wedges. The BBO, calcite and glass wedges are placed after the focusing lens to minimize chromatic aberrations. The IR+SH beam is focused into a continuous-flow gas cell filled with noble-gas atoms (Kr) to generate an APT (XUV 1) composed of odd harmonics only. Here, the SH does not influence the HHG process due to its low intensity and large temporal separation. The XUV and IR+SH are spatially separated by a thin aluminum filter (200nm thickness). All beams are refocused by a curved double-mirror (75cm focal length). The IR+SH are then restored to temporal overlap by a drilled fused silica plate, while fully transmitting XUV 1 through its central hole. All fields enter an interaction cell, allowing non-linear XUV wave-mixing processes involving the IR+SH driving-field. A piezo stage controls the temporal delay Δt between the inner and outer mirror segments

with attosecond resolution. A continuous-flow (Kr) glass nozzle downstream generates a reference APT (XUV 2) from the overlapped IR+SH field, composed of odd and even harmonics. The odd (even) harmonics are polarized along the IR (SH) field. The reference pulses (XUV 2) interfere with the transmitted pulses (Transmitted XUV 1), modified by the non-linear interaction. The XUV-XUV interference is spectrally resolved using a flat-field aberration-corrected concave grating, recorded using a micro-channel plate (MCP) detector and imaged by a charge-coupled device (CCD) camera.

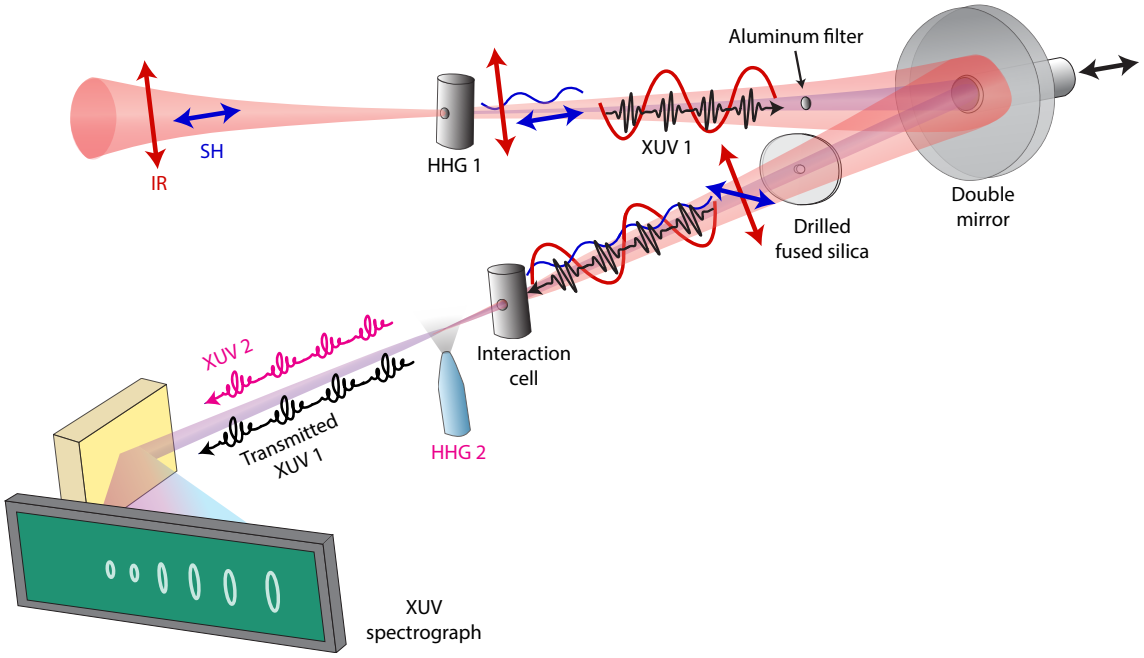

Figure 1. **Experimental setup for vectorial attosecond transient spectroscopy.** A strong IR field and its weak perpendicular second-harmonic (SH) are focused into the a gas cell, where the first attosecond pulse train (APT) is generated. The IR and SH are not temporally overlapped such that only linear odd harmonics (XUV 1) are produced in the first cell. An aluminum filter spatially separates XUV 1. A fused silica window is used to restore temporal overlap between the IR and SH. All fields are refocused into a helium filled interaction cell, inducing non-linear processes. The relative delay Δt between XUV 1 and the two-color field is controlled by a two-segment mirror. A third gas source generates the reference APT (XUV 2), composed of even and odd harmonics with linear and orthogonal polarization states, which interferes with the modified APT (Transmitted XUV 1).

2. QUANTUM PATH AND POLARIZATION STATE ISOLATION

2.1. Effective susceptibility tensor

Non-linear interactions modify the effective XUV complex optical susceptibility. In general, the properties of the target can be manipulated in a vectorial manner via the interaction with a vectorial incoming field $\vec{E}_{in}$. Such a field interacts with the electronic wavefunction of the target, generating non-linear wave-mixing processes. When the interaction is generated in an atomic gas targets, even orders of the susceptibility vanish, reflecting the isotropic nature of the system. Due to these symmetry constrains, the lowest non-linear order of the interaction is a four-wave-mixing mechanism. The generated field in a transient interaction can be approximated by: $\vec{E}_{gen}(\omega) \approx \vec{E}^{(1)}_{gen}(\omega) + \vec{E}^{(3)}_{gen}(\omega)$, where $\vec{E}^{(1)}_{gen}$ and $\vec{E}^{(3)}_{gen}$ are the linear and third-order response, respectively. The incoming field can have the form $\vec{E}_{in} = \vec{E}_{dr}(\Delta t) + \vec{E}_{pr}$, where $\vec{E}_{dr}$ is the vectorial driving-field, in the VIS-IR regime, and $\vec{E}_{pr}$ is the probing attosecond pulses in the XUV spectral regime. Controlling the delay between the two fields, Δt, allows the attosecond pulses to probe the transient interaction. The generated field is proportional to the structural susceptibility tensor of the target[1], $\overleftrightarrow{\chi}$, and the interaction follows:

$$\begin{aligned}\vec{E}_{gen}(\omega,\Delta t) &\approx \vec{E}^{(1)}_{gen}(\omega) + \vec{E}^{(3)}_{gen}(\omega,\Delta t) \\ &= i\omega\xi\chi^{(1)}(\omega)\vec{E}_{pr}(\omega) \\ &+ i\omega\xi \iiint_{\Gamma} d\omega_1 d\omega_2 d\Omega \chi^{(3)}(\omega;\omega_1,\omega_2,\Omega)\vec{E}_{dr}(\omega_1)e^{-i\omega_1\Delta t}\vec{E}_{dr}(\omega_2)e^{-i\omega_2\Delta t}\vec{E}_{pr}(\Omega) \\ &\Gamma : \omega = \omega_1 + \omega_2 + \Omega\end{aligned} \tag{1}$$

with ξ being a proportionality constant, representing the density length product of the interaction cell. The linear and third-order susceptibility terms, $\chi^{(1)}$ and $\chi^{(3)}$, set the optical response up to four-wave-mixing processes. From this equation, we can define an effective susceptibility tensor for the interaction

$$\overleftrightarrow{\chi}^{eff}(\omega,\Omega) \equiv i\omega\xi \int d\omega_1 \chi^{(3)}(\omega;\omega_1,\omega_2,\Omega)\vec{E}_{dr}(\omega_1)\vec{E}_{dr}(\omega_2), \quad \omega_2 = \omega - \omega_1 - \Omega \tag{2}$$

and simplify the expression of the generated field:

$$\vec{E}_{gen}(\omega,\Delta t) \approx i\omega\xi\chi^{(1)}(\omega)\vec{E}_{pr}(\omega) + \int d\Omega \overleftrightarrow{\chi}^{eff}(\omega,\Omega)\vec{E}_{pr}(\Omega)e^{i(\Omega-\omega)\Delta t} \tag{3}$$

The effective susceptibility $\overleftrightarrow{\chi}^{eff}(\omega,\Omega)$ converts an incoming XUV frequency Ω to an outgoing XUV frequency ω, and its tensoric form allows it to rotate polarization. The term $\overleftrightarrow{\chi}^{eff}(\omega,\Omega)e^{i(\Omega-\omega)\Delta t}$ beats with the frequency difference between the incoming and

generated fields, leading to sub-cycle modulations. We can further simplify the equations by accounting for integer harmonic orders, setting

$$\omega = n\omega_{IR}, \quad \Omega = m\omega_{IR}, \quad n, m \in \mathbb{N} \tag{4}$$

and replacing integration over XUV frequencies by a sum:

$$\vec{E}_{gen}(n, \Delta t) \approx i\omega\xi\chi^{(1)}(n)\vec{E}_{pr}(n) + \sum_{m \in m_{odd}} \overleftrightarrow{\chi}^{eff}(n, m)\vec{E}_{pr}(m)e^{i(m-n)\Delta t} \tag{5}$$

The generated field encapsulates the light-driven quantum mechanical processes that are induced in the target. Under the dipole approximation, the spectrum of the macroscopic generated field is proportional to the expectation value of the dipole response[2]:

$$\vec{E}_{gen}(\omega, \Delta t) \propto \vec{D}(\omega, \Delta t), \quad \vec{D}\left(t, \Delta t\right) = \left\langle \psi\left(t, \Delta t\right) \middle| \vec{d} \middle| \psi\left(t, \Delta t\right) \right\rangle \tag{6}$$

where $\vec{d}$ is the dipole operator and $\psi\left(t, \Delta t\right)$ is the electronic quantum wave-function of the sample. Thus, the generated field captures the symmetries of the light-driven electronic wavefunction.

2.2. Channel separation

Applying an interferometric approach, the generated XUV field is interfered with an external reference, to determine its amplitude and phase. Then, the intensity of the signal as function of optical frequency ω and delay Δt is of the form:

$$I(\omega, \Delta t) \approx \left| \vec{E}_{pr}(\omega) + \vec{E}^{(1)}_{gen}(\omega) + \vec{E}^{(3)}_{gen}(\omega, \Delta t) + \vec{E}_{ref}(\omega, \Delta t) \right|^2 \tag{7}$$

capturing the interference term of the generated field with an external reference $\vec{E}_{ref}(\omega, \Delta t) = \vec{E}_{ref}(\omega)e^{-i\omega\Delta t}$. Since $\vec{E}_{pr}$ and $\vec{E}^{(1)}_{gen}$ are not delay dependent, their interference signal with $\vec{E}_{ref}(\omega)e^{-i\omega\Delta t}$ oscillates according to the optical frequency ω and can be separated from the non-linear contribution by Fourier analysis. We focus on the interference term between the non-linear field $\vec{E}^{(3)}_{gen}$ and the reference. Following equation 3, we can define the non-linear interference term:

$$\begin{aligned}
I^{NL}_{int}(\omega, \Delta t) &\equiv \left| \vec{E}^{(3)}_{gen}(\omega, \Delta t) + \vec{E}_{ref}(\omega, \Delta t) \right|^2 && (8)\\
&= \left| \int d\Omega \overleftrightarrow{\chi}^{eff}(\omega, \Omega)\vec{E}_{pr}(\Omega)e^{i(\Omega-\omega)\Delta t} + \vec{E}_{ref}(\omega)e^{-i\omega\Delta t} \right|^2 && (9)\\
&= \left| \int d\Omega \overleftrightarrow{\chi}^{eff}(\omega, \Omega)\vec{E}_{pr}(\Omega)e^{i\Omega\Delta t} + \vec{E}_{ref}(\omega) \right|^2 && (10)\\
&= C(\omega) + (\vec{E}_{ref}(\omega))^* \cdot \int d\Omega \overleftrightarrow{\chi}^{eff}(\omega, \Omega)\vec{E}_{pr}(\Omega)e^{i\Omega\Delta t} + c.c. && (11)
\end{aligned}$$

with $C(\omega) = \left|\vec{E}^{(3)}_{gen}\right|^2 + \left|\vec{E}_{ref}\right|^2$ being a spectral amplitude which does not depend on Δt. This term separates the different non-linear channels, linking an incoming frequency to a transmitted frequency, by taking a Fourier transform with respect to Δt:

$$A^{NL}_{int}(\omega,\nu) \propto (\vec{E}_{ref}(\omega))^* \cdot \int d\Omega \overleftrightarrow{\chi}^{eff}(\omega,\Omega)\vec{E}_{pr}(\Omega)\delta(\Omega-\nu) + c.c. \tag{12}$$

$$= (\vec{E}_{ref}(\omega))^* \cdot \overleftrightarrow{\chi}^{eff}(\omega,\nu)\vec{E}_{pr}(\nu) + c.c. \tag{13}$$

Equation 13 implies that the Fourier map $I_{int}(\omega,\nu)$ is proportional to the effective susceptibility tensor $\overleftrightarrow{\chi}^{eff}(\omega,\nu)$, mapping incoming harmonic with optical frequency ν to a transmitted harmonic with optical frequency ω.

Once again, the expressions can be simplified by considering integer harmonic numbers (see Equation 4). Then, the non-linear interference is

$$I^{NL}_{int}(n,\Delta t) = \left| \sum_{m\in m_{odd}} \overleftrightarrow{\chi}^{eff}(n,m)\vec{E}_{pr}(m)e^{im\omega_{IR}\Delta t} + \vec{E}_{ref}(n) \right|^2 \tag{14}$$

and the complex Fourier map has the form:

$$A^{NL}_{int}(n,m) \propto (\vec{E}_{ref}(n))^* \cdot \overleftrightarrow{\chi}^{eff}(n,m)\vec{E}_{pr}(m) + c.c., \quad m \in m_{odd} \tag{15}$$

2.3. Spectral polarization states of the generated field

For a general driving-field $\vec{E}_{dr}$, the $\hat{a}$ polarization component of the non-linear generated field $\vec{E}^{(3)}_{gen}$ is

$$E^{(3)}_{gen,a}(\omega,\Delta t) = i\omega\xi \sum_{bcd} \iiint_{\Gamma} d\omega_1 d\omega_2 d\Omega \chi^{(3)}_{abcd}(\omega;\Omega,\omega_1,\omega_2) \tag{16}$$

$$\times E_{dr,b}(\omega_1)E_{dr,c}(\omega_2)E_{in,XUV,d}(\Omega)e^{i(\Omega-\omega)\Delta t}$$

$$\Gamma : \omega = \omega_1 + \omega_2 + \Omega$$

where the tensor $\chi^{(3)}_{abcd}$ converts three photons which are $\hat{b}$-,$\hat{c}$- and $\hat{d}$-polarized into one photon with $\hat{a}$-polarization state.

In our experiment, the incoming IR and XUV are $\hat{x}$-polarized, and the incoming SH has the perpendicular $\hat{y}$-polarization. In addition, the incoming XUV is composed of odd harmonics only. Working in the $\hat{x},\hat{y}$ basis, every polarization index in $\chi^{(3)}_{abcd}$ has to appear twice to comply with the original symmetry of the bare atomic system, since a homogeneous system is symmetric under $\hat{x} \to -\hat{x}$ and $\hat{y} \to -\hat{y}$[1]. Therefore, the generated

field of the odd harmonics is:

$$E^{(3)}_{odd,\hat{x}}(\omega,\Delta t) = i\omega\xi \iint d\Omega d\omega_{IR}\chi^{(3)}_{xxxx}(\omega;\Omega,\omega_{IR},\omega-\Omega-\omega_{IR}) \tag{17}$$

$$\times E_{IR,\hat{x}}(\omega_{IR})E_{IR,\hat{x}}(\omega-\Omega-\omega_{IR})E_{in,odd,\hat{x}}(\Omega)e^{i(\Omega-\omega)\Delta t}$$

$$= i\omega\xi \int d\Omega\chi^{eff}_{x\leftarrow x}(\omega,\Omega)\vec{E}_{in,odd}(\Omega)e^{i(\Omega-\omega)\Delta t} \tag{18}$$

$$\chi^{eff}_{x\leftarrow x}(\omega,\Omega) = \int d\omega_{IR}\chi^{(3)}_{xxxx}(\omega;\Omega,\omega_{IR},\omega-\Omega-\omega_{IR})E_{IR,\hat{x}}(\omega_{IR})E_{IR,\hat{x}}(\omega-\Omega-\omega_{IR})$$

where we omit processes of the form χ_{xyyx} which involve more than one SH photon due to the relatively low intensity of the SH field. The contribution of the even harmonics is:

$$E^{(3)}_{even,\hat{y}}(\omega,\Delta t) = i\omega\xi \iint d\Omega d\omega_{SH}\chi^{(3)}_{t}(\omega;\Omega,\omega_{SH},\omega-\Omega-\omega_{SH}) \tag{19}$$

$$\times E_{SH\hat{y}}(\omega_{SH})E_{IR,\hat{x}}(\omega-\Omega-\omega_{SH})E_{odd,in,\hat{x}}(\Omega)e^{i(\Omega-\omega)\Delta t}$$

$$= i\omega\xi \int d\Omega\chi^{eff}_{y\leftarrow x}(\omega,\Omega)\vec{E}_{in,odd}(\Omega)e^{i(\Omega-\omega)\Delta t} \tag{20}$$

$$\chi^{eff}_{y\leftarrow x}(\omega,\Omega) = \int d\omega_{SH}\chi^{(3)}_{t}(\omega;\Omega,\omega_{SH},\omega-\Omega-\omega_{SH})E_{SH\hat{y}}(\omega_{SH})E_{IR,\hat{x}}(\omega-\Omega-\omega_{SH})$$

with $\chi^{(3)}_t = \chi^{(3)}_{yxyx} + \chi^{(3)}_{yyxx}$ converting $\hat{x}$-polarized odd harmonics into $\hat{y}$-polarized even harmonics. To conclude, the original symmetry of the atomic system and the symmetry of the incoming fields define the symmetry of the field-driven system, setting the polarization state of the transmitted harmonics: odd harmonics are $\hat{x}$-polarized, and even harmonics are $\hat{y}$-polarized, as illustrated in Figure 2.

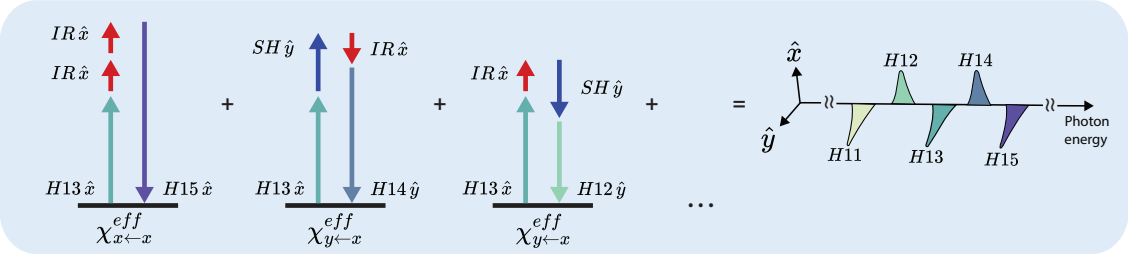

Figure 2. **Vectorial four-wave-mixing processes in the frequency domain.** $\hat{x}$-polarized odd harmonics interact with a symmetric target driven by IR$\hat{x}$+SH$\hat{y}$ field. Selection rules set two types of possible processes: $\chi^{eff}_{x\leftarrow x}$ which generates odd harmonics, or $\chi^{eff}_{y\leftarrow x}$ which generates even harmonics.

3. EXPERIMENTAL DATA AND ANALYSIS

3.1. Complementary measurements

In order to explore the origin of each Fourier peak in the Fourier analysis of vectorial attosecond transient spectroscopy, two additional experiments were conducted: vectorial

attosecond transient absorption (TA) and an interferomentric measurement, performed under identical experimental conditions. The results are presented in Figure 3.

TA is preformed by removing the XUV reference source, probing the amplitude modulations of the transmitted attosecond pulses[3–5]. A train of linearly polarized odd harmonics interact with the helium target driven by the orthogonally polarized two-color field, resolving the spectrum as function of the delay between the incoming XUV and the driving-field, Δt. In such experiment, the appearance of even harmonics would indicate transient nonlinear polarization rotation. However, the generated even harmonics are weak, and cannot be properly detected. TA captures the appearance of harmonic 14, but does not detect harmonic 12, which has a weaker amplitude. The Fourier analysis of these results are shown in 3a. The odd harmonics present $2\omega_{IR}$ oscillations, which are a hallmark of attosecond transient absorption[4,6,7]. The Fourier analysis of the TA measurement contains low Fourier frequency components only for harmonic 14, probing its dynamical properties along a relatively slow time scale, dictated by the envelope of the pulse.

The interferometric experiment is preformed by switching off the intermediate helium gas target. This experiment interferes the attosecond pulses of both HHG sources[8–11]. The first HHG source produces a train of linearly polarized attosecond pulses, composed of odd harmonics only. The second HHG source produces vectorial attosecond pulses, even and odd harmonics with linear and perpendicular polarization states. The Fourier analysis of the interferometric experiment is presented in Figure 3b. The Fourier map shows that the odd harmonics oscillate according to their photon frequency and the even harmonics do not have any XUV Fourier peaks. All harmonics present $1\omega_{IR}$ oscillations with respect to the delay. These oscillations appear due to a minor IR leak through the aluminum filter. Scanning the delay causes a residual IR-IR interference in the second HHG source, which slightly perturbs the harmonic yield. This experimental artifact is fully separated by a Fourier analysis.

In the third step we combine the two measurements and resolve vectorial attosecond transient spectroscopy. Figure 3c shows the map of this Fourier analysis. On the lower part of the Fourier spectrum, vectorial attosecond transient spectroscopy captures the $2\omega_{IR}$ oscillations of attosecond transient absorption, along with the $1\omega_{IR}$ experimental artifact of the interferometric experiment. The higher XUV part of the spectrum presents the interferometric peaks of the odd harmonics, accompanied by $2\omega_{IR}$ sidebands, which indicate amplitude and phase modulations to the harmonics, applied by the four-wave-mixing processes. For the even harmonics, simple Fourier analysis with no spectral averaging cap-

tures $13\omega_{IR}$ oscillations, indicating that harmonic 13 contributed to the generation of both harmonic 12 and harmonic 14. Vectorial attosecond transient spectroscopy can identify the incoming harmonics that were involved in transient non-linear polarization rotation, probing the sub-cycle dynamics of this ultrafast mechanism. In addition, this experiment allows the detection of weak signal, which is inaccessible without a lock-in detection.

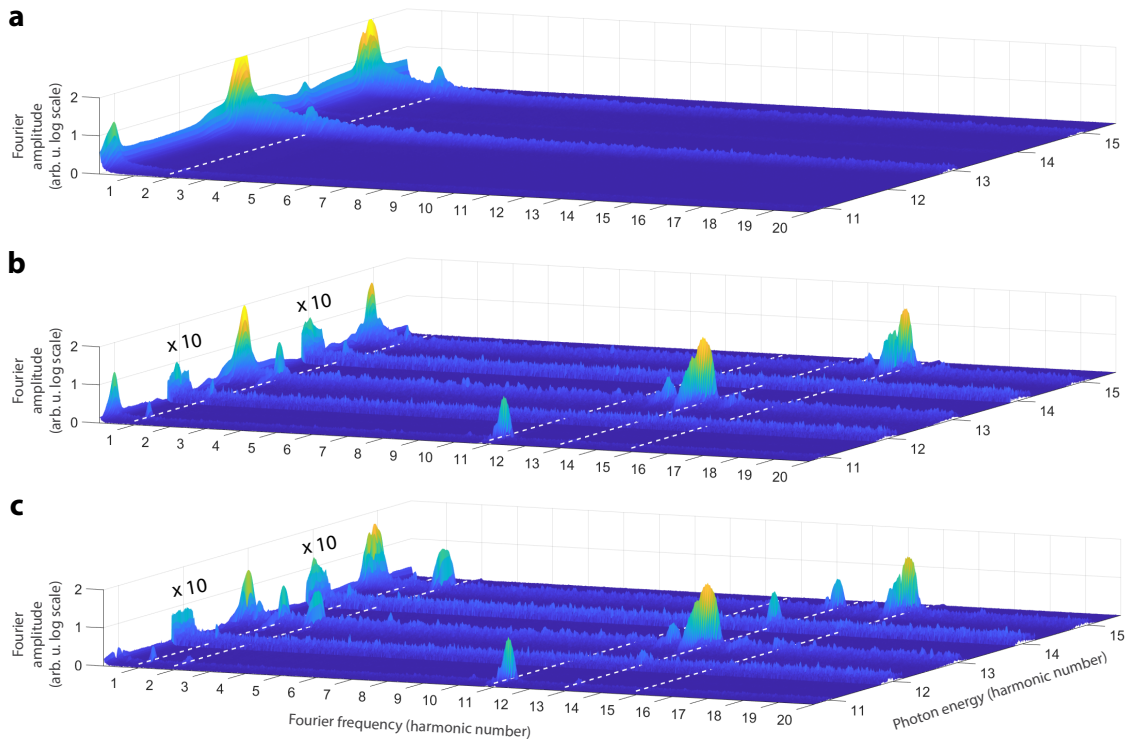

Figure 3. **Experimental results of transient absorption (TA), interferometry and vectorial attosecond transient spectroscopy.** The results are presented with spatial averaging only. **(a)** Fourier analysis of TA. Harmonic 13 and harmonic 15 show $2\omega_{IR}$ absorption oscillations. Harmonic 12 does not appear, and harmonic 14 shows only DC response. **(b)** Fourier analysis of an interferometric experiment, switching off the gas in the helium target. The even harmonic signal is $\times 10$ magnified. Strong interferometric oscillations are shown for the odd harmonics, some accompanied by $1\omega_{IR}$ sidebands, which follow the modulations of the reference. The even harmonics do not have signal in the XUV Fourier frequency regime. **(c)** Fourier analysis of vectorial attosecond transient spectroscopy. The even harmonic signal is $\times 10$ magnified. All features of both TA and the interferometric experiment appear. Odd harmonics present $2\omega_{IR}$ sidebands, for example sideband 15 in harmonic 13 and sideband 13 in harmonic 15. Both even harmonics present $13\omega_{IR}$ oscillations, with no spectral averaging.

3.2. Data analysis

In order to enhance the visibility of the oscillations (see Figure 2 in the main text), an additional Fourier analysis with respect to the delay was applied. Preforming Fourier transform of the experimental data with respect to Δt isolates the relevant Fourier frequencies for each transmitted photon energy. We normalize each optical frequency by its DC Fourier component and apply a Fourier filter around the $2\omega_{IR}$ peaks, the positive interferometric components and their $2\omega_{IR}$ sidebands. The Fourier filter has a spectral range of $\pm$0.155eV-0.465eV ($\pm$0.1-0.3 harmonic number) around the relevant frequency components to fully include all the selected Fourier peaks. Then, we preform inverse Fourier transform with respect to Δt, using the analytic signal analysis method[12,13]. This filtering increases the signal-to-noise ratio and avoids experimental artifacts.

Next, we apply both spatial and spectral averaging to the harmonics, presenting their one-dimensional Fourier components in Figure 3 in the main text. This analysis further increases the signal-to-noise ratio, allowing to capture additional Fourier peaks of harmonic 14 ($11\omega_{IR}$ and $15\omega_{IR}$). In this analysis, we chose for each harmonic a spatial and spectral region with sufficient Fourier amplitude and a flat phase for as many Fourier components as possible. The results are shown in Figure 4. Harmonics 11 and 13 present clear interferometric envelopes, accompanied by weaker beating pattern. Harmonic 12 presents a much weaker signal, oscillating with $13\omega_{IR}$ periodicity, recording the coherent contribution of harmonic 13 in the formation of harmonic 12. These oscillations are a signature of ultrafast non-linear polarization rotation, as the incoming harmonic 13 has $\hat{x}$-polarization, and the transmitted harmonic 12 has $\hat{y}$-polarization. Harmonic 15 and harmonic 14 are both presented in the two-dimensional spectrograms in the main text (Figure 2). The one-dimensional representation of these harmonics highlights two important aspects. First, both harmonics present beating pattern, a signature of the interference between multiple quantum paths, separated in the main text in Figure 3. The second aspect is the absorption of harmonic 15 and emission of harmonic 14 that appear outside of the interferometric envelope, around $\Delta t = 40$fs. These dynamics are associated with the helium 1s3p resonance ($\sim$23.1eV)[14], that lies within the bandwidth of harmonic 15. Harmonic 15 contributes to the transmission of harmonic 14, correlating the absorption feature in harmonic 15 to the emission of harmonic 14 via perturbed free induction decay[15–17].

In attosecond transient interferometry, the waveform of each transmitted harmonic is encoded in the interference term between the generated field and the reference, which includes the interferometric peaks and their sidebands in Fourier domain[18]. To illustrate

the waveform, only these Fourier peaks were isolated with a filter (±0.155eV around each Fourier component). Then, we preform an additional inverse Fourier transform at a fixed Δt, projecting the measured harmonics into the time domain. We illustrate the temporal evolution of the transmitted APT by assigning linear and orthogonal polarization states to odd and even harmonics. The reconstruction is presented in Figure 3a in the main text.

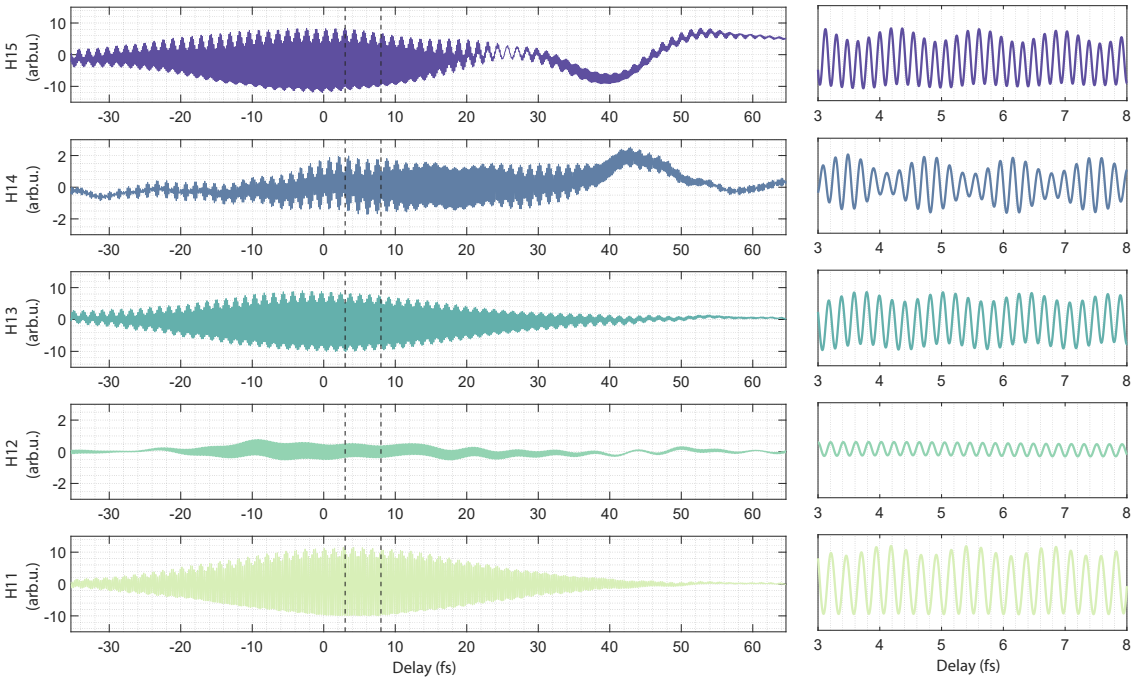

Figure 4. **Vectorial attosecond transient spectroscopy interference signal.** The results are DC normalized and presented with both spatial and spectral averaging. The oscillations of the odd harmonics are modified by the non-linear interaction, reflected by a beating pattern. Even harmonics present oscillations that capture generated field components which rotate the polarization of the incoming APT. Harmonic 15 and harmonic 14 show absorption and emission around $\Delta t = 40$fs, which can be associated with perturbed free induction decay.

4. DYNAMICAL STOKES PARAMETERS

The Stokes parameters provide a complete representation of the polarization state of light. These parameters are a set of four values, including intensity (S_0), the degree of linear polarization (S_1 and S_2), and circular polarization (S_3). The Stokes parameters are widely used to describe and analyze polarization states[19].

The monochromatic Stokes parameters for a complex field $\vec{E}(t) = \vec{E}(\omega)e^{-i\omega t}$ can be

defined as:

$$
\begin{aligned}
S_0 &= |E_x|^2 + |E_y|^2 = |E_a|^2 + |E_b|^2 = |E_l|^2 + |E_r|^2 \\
S_1 &= |E_x|^2 - |E_y|^2 \\
S_2 &= |E_a|^2 - |E_b|^2 \\
S_3 &= |E_r|^2 - |E_l|^2
\end{aligned}
\tag{21}
$$

with the basis vectors

$$
\hat{a} = \frac{1}{\sqrt{2}}\left(\hat{x} + \hat{y}\right), \hat{b} = \frac{1}{\sqrt{2}}\left(\hat{x} - \hat{y}\right); \quad \hat{l} = \frac{1}{\sqrt{2}}\left(\hat{x} + i\hat{y}\right), \hat{r} = \frac{1}{\sqrt{2}}\left(\hat{x} - i\hat{y}\right) \tag{22}
$$

expressed in the $\{\hat{x}, \hat{y}\}$ basis. S_0 is the intensity of the field, and therefore can be calculated by the summation over the squared value of any orthonormal basis. The other Stokes parameters account for the intensity difference between different orthogonal polarization components. S_1 shows the difference between the $\hat{x}$-component and the $\hat{y}$-component. S_2 represents the tilt orientation of the field, and S_3 reveals the handedness, comparing between right- and left-circular polarization intensity components ($\hat{r}$ and $\hat{l}$, respectively). Representing the Stokes parameters in the $\{\hat{x}, \hat{y}\}$ basis, the expressions become:

$$
\begin{aligned}
&S_0 = |E_x|^2 + |E_y|^2, \; S_1 = |E_x|^2 - |E_y|^2 \\
&S_2 = 2Re\left[E_x E_y^*\right], \; S_3 = -2Im\left[E_x E_y^*\right]
\end{aligned}
\tag{23}
$$

where the asterisk denotes complex conjugation.

To describe the vectorial properties of a complex multi-color field $\vec{E}(t) = \int_0^\infty \vec{E}(\omega) e^{-i\omega t} d\omega$, we need to consider its second-order correlations. In our experiment, such an analysis is necessary since the coherent superposition of the bilinear harmonics sets the temporal polarization state of the transmitted attosecond pulses. In the spectral domain, the polarization properties are fully described by the cross-spectral density matrix (CSDM)[20]. The two-frequency CSDM for coherent fields is:

$$
W_{ij}(\omega_1, \omega_2) = E_i^*(\omega_1) E_j^T(\omega_2) \tag{24}
$$

where $i, j \in \{\hat{x}, \hat{y}\}$ denote the linear polarization components and W is Hermitian, $W^*(\omega_2, \omega_1) = W(\omega_1, \omega_2)$. Then, the spectral two-frequency Stokes parameters are

$$
\begin{aligned}
S_0(\omega_1, \omega_2) &= W_{xx}(\omega_1, \omega_2) + W_{yy}(\omega_1, \omega_2) = E_x^*(\omega_1) E_x(\omega_2) + E_y^*(\omega_1) E_y(\omega_2) \\
S_1(\omega_1, \omega_2) &= W_{xx}(\omega_1, \omega_2) - W_{yy}(\omega_1, \omega_2) = E_x^*(\omega_1) E_x(\omega_2) - E_y^*(\omega_1) E_y(\omega_2) \\
S_2(\omega_1, \omega_2) &= W_{xy}(\omega_1, \omega_2) + W_{yx}(\omega_1, \omega_2) = E_x^*(\omega_1) E_y(\omega_2) + E_y^*(\omega_1) E_x(\omega_2) \\
S_3(\omega_1, \omega_2) &= i(W_{yx}(\omega_1, \omega_2) - W_{xy}(\omega_1, \omega_2)) = i(E_y^*(\omega_1) E_x(\omega_2) - E_x^*(\omega_1) E_y(\omega_2))
\end{aligned}
\tag{25}
$$

and their relation to the time domain is:

$$S_j(t) = \int\int S_j(\omega_1, \omega_2) e^{i(\omega_1 - \omega_2)t} d\omega_1 d\omega_2 \tag{26}$$

Each polarization axis j satisfies $E_j(t) = \int_0^\infty E_j(\omega) e^{-i\omega t} d\omega$, and we can describe the polarization of the transmitted attosecond pulses by integrating over ω_1, ω_2 separately. For example, the ellipticity parameter $S_3(t)$ can be expressed as

$$\begin{aligned} S_3(t) &= \int\int S_3(\omega_1, \omega_2) e^{i(\omega_1 - \omega_2)t} d\omega_1 d\omega_2 \\ &= \int\int i(E_y^*(\omega_1) E_x(\omega_2) - E_x^*(\omega_1) E_y(\omega_2)) e^{i(\omega_1 - \omega_2)t} d\omega_1 d\omega_2 \\ &= \int\int i(E_y^*(\omega_1) e^{i\omega_1 t} E_x(\omega_2) e^{-i\omega_2 t} - E_x^*(\omega_1) e^{i\omega_1 t} E_y(\omega_2) e^{-i\omega_2 t}) d\omega_1 d\omega_2 \\ &= i(E_y^*(t) E_x(t) - E_x^*(t) E_y(t)) \\ &= -2Im\left[E_x(t) E_y^*(t)\right] \end{aligned} \tag{27}$$

and similar expressions can be obtained for the other time-depended Stokes parameters:

$$\begin{aligned} &S_0 = |E_x(t)|^2 + |E_y(t)|^2\,,\ S_1 = |E_x(t)|^2 - |E_y(t)|^2 \\ &S_2 = 2Re\left[E_x(t) E_y(t)^*\right],\ S_3 = -2Im\left[E_x(t) E_y(t)^*\right] \end{aligned} \tag{28}$$

The reconstruction of the experimental Stokes parameters is obtained by preforming an inverse Fourier transform to the experimental results along the photon frequency ω, at a given delay time Δt, assuming a flat spectral phase for the reference field. Thus, we can use equation 28 to present the dynamical polarization state, accounting for the temporal evolution of different optical frequencies. The reconstructed dynamical Stokes parameters are shown in Figure 3b in the main text. The complex field of the transmitted harmonics below helium ionization threshold follows:

$$\begin{aligned} E_x &= A_{11}(t) e^{i11\omega_{IR}t + i\phi_{11}(t)} + A_{13}(t) e^{i13\omega_{IR}t + i\phi_{13}(t)} + A_{15}(t) e^{i15\omega_{IR}t + i\phi_{15}(t)} \\ E_y &= A_{12}(t) e^{i12\omega_{IR}t + i\phi_{12}(t)} + A_{14}(t) e^{i14\omega_{IR}t + i\phi_{14}(t)} \end{aligned} \tag{29}$$

where ω_{IR} is the central frequency of the IR field, and with amplitude and phase functions $A_j(t), \phi_j(t)$ that evolve on a multi-cycle timescale, determined by the temporal envelope of the fundamental field. In this case, the dynamics of the Stokes parameters will be dominated by:

$$\begin{aligned} S_0, S_1 &\propto e^{i2\omega_{IR}t}, e^{i4\omega_{IR}t} \\ S_2, S_3 &\propto e^{i\omega_{IR}t}, e^{i3\omega_{IR}t} \end{aligned} \tag{30}$$

The expressions for the total intensity (S_0) and the difference between $\hat{x}$ and $\hat{y}$ intensities (S_1) do not couple E_x and E_y and thus oscillate at even orders of ω_{IR}. The orientation (S_2) and handedness (S_3) capture the interplay between E_x and E_y, which changes substantially by their relative phase. Therefore, these dynamical Stokes parameters oscillate at odd orders of ω_{IR}. The temporal evolution of the polarization state, captured by the dynamical Stokes parameters, reflects the dynamical symmetries of the field-driven system which evolves on a sub-cycle timescale.

[1] Robert W. Boyd. *Nonlinear Optics, 4th Edition*. Academic Press, March 2020.

[2] JC Baggesen, Eva Lindroth, and LB Madsen. Theory of attosecond absorption spectroscopy in krypton. *Physical Review A*, 85(1):013415, 2012.

[3] M Holler, F Schapper, L Gallmann, and Ursula Keller. Attosecond electron wave-packet interference observed by transient absorption. *Physical review letters*, 106(12):123601, 2011.

[4] Shaohao Chen, M Justine Bell, Annelise R Beck, Hiroki Mashiko, Mengxi Wu, Adrian N Pfeiffer, Mette B Gaarde, Daniel M Neumark, Stephen R Leone, and Kenneth J Schafer. Light-induced states in attosecond transient absorption spectra of laser-dressed helium. *Physical Review A*, 86(6):063408, 2012.

[5] Michael Chini, Baozhen Zhao, He Wang, Yan Cheng, SX Hu, and Zenghu Chang. Subcycle ac stark shift of helium excited states probed with isolated attosecond pulses. *Physical review letters*, 109(7):073601, 2012.

[6] Mengxi Wu, Shaohao Chen, Seth Camp, Kenneth J. Schafer, and Mette B. Gaarde. Theory of strong-field attosecond transient absorption. *Journal of Physics B: Atomic, Molecular and Optical Physics*, 49(6):062003, February 2016.

[7] Jørgen Johansen Rørstad, Jens E. Bækhøj, and Lars Bojer Madsen. Analytic modeling of structures in attosecond transient-absorption spectra. *Physical Review A*, 96(1):013430, July 2017.

[8] Doron Azoury, Omer Kneller, Shaked Rozen, Barry D Bruner, Alex Clergerie, Yann Mairesse, Baptiste Fabre, Bernard Pons, Nirit Dudovich, and Michael Krüger. Electronic wavefunctions probed by all-optical attosecond interferometry. *Nature Photonics*, 13(1):54, 2019.

[9] Doron Azoury, Omer Kneller, Michael Krüger, Barry D Bruner, Oren Cohen, Yann Mairesse, and Nirit Dudovich. Interferometric attosecond lock-in measurement of extreme-ultraviolet circular dichroism. *Nature Photonics*, 13(3):198, 2019.

[10] Omer Kneller, Doron Azoury, Yotam Federman, Michael Krüger, Ayelet J Uzan, Gal Orenstein, Barry D Bruner, Olga Smirnova, Serguei Patchkovskii, Misha Ivanov, et al. A look under the tunnelling barrier via attosecond-gated interferometry. *Nature photonics*, 16(4):304–310, 2022.

[11] Michael Krüger and Nirit Dudovich. Attosecond Interferometry. In Kiyoshi Ueda, editor, *Ultrafast Electronic and Structural Dynamics*, pages 45–71. Springer Nature, Singapore, 2024.

[12] A. Reilly, G. Frazer, and B. Boashash. Analytic signal generation-tips and traps. *IEEE Transactions on Signal Processing*, 42(11):3241–3245, 1994.

[13] Maans Klingspor. Hilbert transform: Mathematical theory and applications to signal processing, 2015.

[14] J.R.Fuhr W.L.Wieseand. Accurate atomic transition probabilities for hydrogen, helium, and lithium. *NIST databese*, January 2009.

[15] Alexander Blättermann, Christian Ott, Andreas Kaldun, Thomas Ding, and Thomas Pfeifer. Two-dimensional spectral interpretation of time-dependent absorption near laser-coupled res-

onances. *Journal of Physics B: Atomic, Molecular and Optical Physics*, 47(12):124008, June 2014.

[16] Christian Ott, Andreas Kaldun, Luca Argenti, Philipp Raith, Kristina Meyer, Martin Laux, Yizhu Zhang, Alexander Blättermann, Steffen Hagstotz, Thomas Ding, Robert Heck, Javier Madroñero, Fernando Martín, and Thomas Pfeifer. Reconstruction and control of a time-dependent two-electron wave packet. *Nature*, 516(7531):374–378, December 2014.

[17] S. Beaulieu, E. Bloch, L. Barreau, A. Comby, D. Descamps, R. Géneaux, F. Légaré, S. Petit, and Y. Mairesse. Phase-resolved two-dimensional spectroscopy of electronic wave packets by laser-induced XUV free induction decay. *Physical Review A*, 95(4):041401, April 2017.

[18] Omer Kneller, Chen Mor, Nikolai D. Klimkin, Noa Yaffe, Michael Krüger, Doron Azoury, Ayelet J. Uzan-Narovlansky, Yotam Federman, Debobrata Rajak, Barry D. Bruner, Olga Smirnova, Serguei Patchkovskii, Yann Mairesse, Misha Ivanov, and Nirit Dudovich. Attosecond transient interferometry. *Nature Photonics*, pages 1–8, November 2024. Publisher: Nature Publishing Group.

[19] Eugene Hecht. *Optics, 5th Edition*. Pearson, 2017.

[20] Jari Turunen and Frank Wyrowski. Time-dependent physical stokes parameters and degree of polarization of light. *Phys. Rev. A*, 99:023824, Feb 2019.